

An adaptive-recursive staggering strategy for simulating multifield coupled processes in microheterogeneous solids

T. I. Zohdi^{*,†}

*Institut für Baumechanik und Numerische Mechanik, Universität Hannover, Appelstrasse 9A,
30167 Hannover, Germany*

SUMMARY

In this work an adaptive-recursive staggering strategy is developed for the solution of partial differential equations arising from descriptions of multifield coupled processes in microheterogeneous solids. In order to illustrate the solution strategy, a multifield model problem is studied which describes the diffusion of a detrimental dilute solute into a solid material. The coupled equations to be solved are (1) a phenomenological diffusion-reaction equation, (2) a phenomenological damage evolution law, (3) a balance of energy, and (4) a balance of momentum. The finite element method is used for the spatial discretization, and finite differences for the temporal discretization. In order to accurately capture the microstructure of the material, use of very fine finite element meshes is inescapable. Therefore, in order to reduce computation time, one would like to take as large time steps as possible, provided that the associated numerical accuracy can be maintained. Classical staggering approaches solve each field equation in an uncoupled manner, by allowing only the primary field variable to be active, and momentarily freezing all others. After the solution of each field equation, the primary field variable is updated, and the next field equation is treated in a similar manner. In standard approaches, after this process has been applied, only once, to all of the field equations, the time step is immediately incremented. This non-recursive process is highly sensitive to the order in which the staggered field equations are solved. Furthermore, since the staggering error accumulates with each passing time step, the process may require very small time steps for sufficient accuracy. In the approach developed here, in order to reduce the error within a time step, the staggering methodology is formulated as a recursive fixed-point iteration, whereby the system is repeatedly re-solved until fixed-point type convergence is achieved. A sufficient condition for the convergence of such a fixed-point scheme is that the spectral radius of the coupled operator, which depends on the time step size, must be less than unity. This observation is used to adaptively maximize the time step sizes, while simultaneously controlling the coupled operator's spectral radius, in order to deliver solutions below an error tolerance within a prespecified number of desired iterations. This recursive staggering error control allows substantial reduction of computational effort by the adaptive use of large time steps. Three-dimensional numerical examples are given to illustrate the approach. Copyright © 2001 John Wiley & Sons, Ltd.

KEY WORDS: staggering schemes; multifield systems; microheterogeneous materials

*Correspondence to: T. I. Zohdi, Department of Civil Engineering, University of Hannover, Appelstr. 9A, 30167 Hannover, Germany

†E-mail: zohdi@ibnm.uni-hannover.de

1. INTRODUCTION

It is estimated that in the United States and Europe approximately 60 billion dollars are spent yearly to protect against and repair various forms of chemical damage to structural materials. Accordingly, due to the time consuming and expensive nature of laboratory experiments, one area of high industrial interest is the numerical simulation of chemical damage in materials exposed to aggressive environments. A class of engineering materials of wide interest are those formed by a homogeneous matrix containing a dispersed phase of particulate heterogeneities of different properties. In the construction of such materials, the usual philosophy is to select material combinations to produce aggregate responses possessing desirable properties from each component. For example, in structural engineering applications, the classical choice is a harder particulate phase that serves as a stiffener for the base matrix material. Such inhomogeneities are encountered in metal matrix composites, concrete, etc (Figure 1).

The typical structural engineering approach to characterize the aggregate or macroscopic mechanical response is via a relation between averages $\langle \boldsymbol{\sigma} \rangle_{\Omega} = \mathbb{E}^* : \langle \boldsymbol{\varepsilon} \rangle_{\Omega}$, where \mathbb{E}^* is known as the effective property, and where $\langle \cdot \rangle_{\Omega} \stackrel{\text{def}}{=} 1/|\Omega| \int_{\Omega} \cdot d\Omega$, and $\boldsymbol{\sigma}$ and $\boldsymbol{\varepsilon}$ are the stress and strain tensor fields within a statistically representative volume element of volume $|\Omega|$. For reviews of this classical topic, the reader is referred to Jikov *et al.* [1] for mathematical aspects and to Aboudi [2], Mura [3] or Nemat-Nasser and Hori [4] for mechanically inclined accounts. Despite many of the advantageous structural attributes of such microheterogeneous materials, they can be extremely vulnerable to chemical damage due to (1) the amplified and highly irregular internal stress fields and (2) the strongly contrasting transport properties within the material microstructure, which can result in the internal buildup of diffusing detrimental chemicals. There are many types of chemical degradation that engineering structures can experience, and it would be futile, and beyond the scope of this work, to attempt to analyse them all. However, a relatively general series of interacting (coupled) events are (1) the thermally dependent diffusion of a detrimental dilute solute into a solid material, (2) reactions between the solute and the solid, resulting in damage to the solid, (3) a release of heat and energy transfer in the solid, and

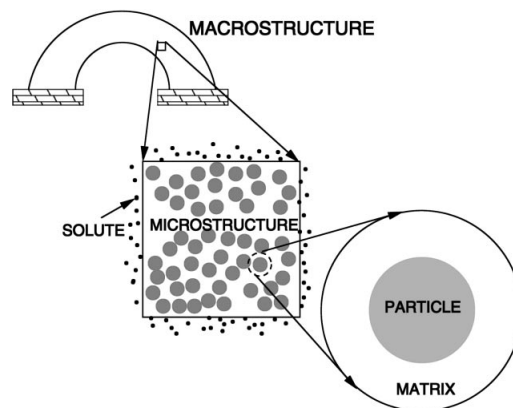


Figure 1. A model problem of a microheterogeneous solid material with a chemical solute on its surface, capable of diffusing into the interior.

(4) a change in the internal stress state in the solid. *The concern of this work is in developing solution techniques for solving coupled partial differential equations arising from multifield processes, such as (1)–(4), in microheterogeneous solids.*

Following the usual approach, the spatial discretization of the heterogeneous microstructure is achieved by the finite element method, while finite differences are used for the temporal discretization. For this class of problems, in order to accurately capture the microstructure, one must use extremely fine finite element meshes. Therefore, in order to reduce computation time, one would like to take as large time steps as possible, provided that associated numerical accuracy can be controlled. A popular class of multifield solution techniques are so-called ‘staggering schemes’, whereby, within a time step, each field equation is solved individually, allowing only the primary field variable to be active. After the solution of each field equation, the primary field variable is updated, and the next field equation is addressed in a similar manner. In the standard approach, after this process has been applied, only once, to all of the field equations, the time step is incremented and the procedure is repeated. The classical solution process is non-recursive, and is highly sensitive to the order in which the field variables are staggeredly solved. The order of staggering is usually selected based upon somewhat ad hoc arguments pertaining to which field ‘drives’ the other. For example for a weakly coupled thermo-mechanical problem, within a time step, one might first solve for the thermal field, using the displacement field from the previous time step as given data, thereafter using the solved for thermal field as a given load in the balance of momentum to solve for an updated value of the displacement field. Thereafter, the time step would be incremented, and the process repeated. For accurate numerical solutions, such approaches requires small time steps, primarily because the staggering error accumulates with each passing increment. For details, see References [5–9]. A particularly lucid review can be found in Reference [10]. A further primary problem is when there are multiple fields with complicated coupling, it is extremely difficult to ascertain in what order to stagger the solution process. Furthermore, as time progresses, for complicated systems, the coupling can change, becoming stronger, weaker or oscillatory. *In an attempt to improve upon such classical staggering approaches for multifield systems where the coupling is difficult to ascertain a-priori, in the present work, a recursive solution strategy is developed, which allows the adaptive use of large or small time steps.*

The outline of the work is as follows. In Section 2, the field equations for a phenomenologically based multifield model problem are developed. In Section 3, a staggering solution strategy is developed whereby, within a time step, each field equation is solved allowing only the primary field variable to be active. All other field variables are momentarily frozen. After the solution of the uncoupled field equation, the active variable is updated, and the process is applied to the next field equation. The procedure is repeatedly applied to the entire multifield system of equations until fixed-point type convergence is achieved. The recursive, self-correcting, nature of the solution process reduces the sensitivity, with respect to classical non-recursive approaches, to the order of equation staggering. A sufficient condition for the convergence of such a fixed-point scheme is that the spectral radius of the coupled operator, which depends on the time step size, must be less than one. This crucial observation is used to adaptively maximize the time step sizes, while simultaneously controlling the associated fixed-point iteration operator’s spectral radius, in order to meet an error tolerance in a pre-specified number of desired iterations. Employing these concepts, a solution strategy, capable of delivering accurate solutions at a fraction of the cost of a typical non-recursive small step

staggering scheme, is developed. In Section 4, three-dimensional numerical examples involving large samples of microheterogeneous particulate solids are given to illustrate the solution technique. In Section 5, some concluding remarks are given.

2. A PHENOMENOLOGICAL MODEL PROBLEM

A structure which occupies an open bounded domain in $\Omega \in \mathbb{R}^3$, with boundary $\partial\Omega$, is considered. The boundary consists of (1) Γ_c and Γ_G , where the solute concentrations (c) and solute fluxes are, respectively, specified, (2) Γ_u on which the displacements (\mathbf{u}) are prescribed and a part Γ_t on which tractions are prescribed, and (3) Γ_θ on which the temperature (θ) is prescribed, and a part Γ_q on which thermal fluxes are prescribed. The mechanical, thermal, and diffusive properties of the heterogeneous material are characterized by a spatially varying elasticity tensor $\mathbb{E} \in \mathbb{R}^{3^2 \times 3^2}$, a spatially varying conductivity tensor $\mathbb{K} \in \mathbb{R}^{3 \times 3}$, and a spatially varying diffusivity tensor $\mathbb{D}^0 \in \mathbb{R}^{3 \times 3}$, all of which are assumed to be symmetric bounded positive definite tensor functions. For example for the elasticity tensor $\forall \boldsymbol{\varepsilon} \in \mathbb{R}^{3 \times 3}$, $\boldsymbol{\varepsilon} = \boldsymbol{\varepsilon}^T$, $a_+ \boldsymbol{\varepsilon} : \boldsymbol{\varepsilon} \geq \boldsymbol{\varepsilon} : \mathbb{E} : \boldsymbol{\varepsilon} \geq a_- \boldsymbol{\varepsilon} : \boldsymbol{\varepsilon}$, $\infty > a_- , a_+ > 0$, $\forall \mathbf{x} \in \Omega$, where $E_{ijkl}(\mathbf{x}) = E_{jikl}(\mathbf{x}) = E_{ijlk}(\mathbf{x}) = E_{klji}(\mathbf{x})$, $1 \leq i, j, k, l \leq 3$, $E_{ijkl}(\mathbf{x})$ being the Cartesian components of \mathbb{E} at point \mathbf{x} . Following standard notation, $H^1(\Omega)$ denotes the usual space of functions with generalized partial derivatives of order ≤ 1 in $L^2(\Omega)$. The notation $\mathbf{H}^1(\Omega) \stackrel{\text{def}}{=} [H^1(\Omega)]^3$ indicates a space of vector-valued functions whose components have generalized partial derivatives of order ≤ 1 in $L^2(\Omega) \stackrel{\text{def}}{=} [L^2(\Omega)]^3$. The symbol ' $\mathbf{u}|_{\partial\Omega}$ ', is used to denote boundary values, for example of the displacement. It is assumed that the boundary data are $L^2(\partial\Omega)$ admissible, however, less smooth data can be considered without complications. For reasons of clarity, strong forms are used to derive the governing equations, assuming more regularity than possible. Afterwards, only the weak forms, which produce solutions which coincide with strong form solutions when the solution is smooth enough, are employed.

2.1. A phenomenological diffusion-reaction equation

The mass balance for a small diffusing species, denoted by the normalized concentration of the solute c (molecules per unit volume), in an arbitrary subvolume of material contained within Ω , denoted ω , consists of a storage term (\dot{c}), a reaction term (\dot{s}), and an inward normal flux term ($-\mathbf{G} \cdot \mathbf{n}$), leading to $\int_{\omega} (\dot{c} + \dot{s}) d\omega = - \int_{\partial\omega} \mathbf{G} \cdot \mathbf{n} da$. A standard stoichiometrically inexact approximation is to assume that the diffusing species reacts (is created or destroyed) in a manner such that the rate of production of the reactant (s) is directly proportional to the concentration of the diffusing species itself, $\dot{s} = \tau c$ and $\tau = \tau^0 e^{-Q/R\theta}$, where τ^0 is a rate constant, Q is an activation energy per mole of diffusive species and where R is the universal gas constant and θ is the temperature. When $\tau^0 > 0$, the diffusing species is destroyed as it reacts, while $\tau^0 < 0$ means that the diffusing species is created as it reacts, i.e. an autocatalytic or 'chain' reaction occurs. Upon substitution of these relations into the conservation law for the diffusing species, and after using the divergence theorem, since the volume ω is arbitrary, one has the usual diffusion-reaction model in strong form

$$\dot{c} = \nabla \cdot (\mathbb{D} \cdot \nabla c) - \tau c \quad (1)$$

where the familiar Arrhenius form $\mathbb{D} = \mathbb{D}_0 e^{-U/R\theta}$ has been used, where \mathbb{D}_0 is the diffusivity tensor (area per unit time) at a reference temperature and where U is the activation energy for solute motion per mole of diffusive species. For details see References [11–13].

2.2. An energy balance

The interconversions of mechanical, thermal and chemical energy are governed by the first law of thermodynamics, where the time rate of change of the total energy, $\mathcal{K} + \mathcal{I}$, is equal to the work rate, \mathcal{P} , and the net heat supplied, $\mathcal{H} + \mathcal{Q}$, i.e. $d/dt(\mathcal{K} + \mathcal{I}) = \mathcal{P} + \mathcal{H} + \mathcal{Q}$. Here the kinetic energy of the subvolume of material contained Ω , denoted ω , is $\mathcal{K} \stackrel{\text{def}}{=} \int_{\omega} \frac{1}{2} \rho \dot{\mathbf{u}} \cdot \dot{\mathbf{u}} d\omega$, the rate of work or power of external volumetric ($\rho \mathbf{b}$) and surface ($\boldsymbol{\sigma} \cdot \mathbf{n}$) forces acting on ω is given by $\mathcal{P} \stackrel{\text{def}}{=} \int_{\omega} \rho \mathbf{b} \cdot \dot{\mathbf{u}} d\omega + \int_{\partial\omega} \boldsymbol{\sigma} \cdot \mathbf{n} \cdot \dot{\mathbf{u}} da$, the heat flow into the volume by conduction is $\mathcal{Q} \stackrel{\text{def}}{=} - \int_{\partial\omega} \mathbf{q} \cdot \mathbf{n} da = - \int_{\omega} \nabla \cdot \mathbf{q} d\omega$, the heat generated due to sources, such as chemical reactions, is $\mathcal{H} \stackrel{\text{def}}{=} \int_{\omega} \rho z d\omega$ and the stored energy is $\mathcal{I} \stackrel{\text{def}}{=} \int_{\omega} \rho w d\omega$. The presence of the dilute diffusing species is modeled phenomenologically, by assuming that it reacts and changes the solid, resulting in a production or consumption of heat. In the present work, the density of the diffusing species is assumed to be negligible compared to that of the solid. Accordingly, making the approximation that the mass in the solid is approximately constant, one has that, the current solid mass $= \int_{\omega} \rho d\omega = \int_{\omega_0} \rho J d\omega_0 \approx \int_{\omega_0} \rho_0 d\omega_0 = \text{the original solid mass}$, and one obtains $\rho J = \rho_0$, which implies $\dot{\rho} J + \rho \dot{J} = 0$. Using the previous relations, a balance of momentum, and the fact that the volume ω is arbitrary, leads to the following local form:

$$\rho \dot{w} - \boldsymbol{\sigma} : \nabla \dot{\mathbf{u}} + \nabla \cdot \mathbf{q} - \rho z = 0 \quad (2)$$

For more details see Reference [10].

2.3. Constitutive assumptions

In this analysis, only infinitesimal strains are considered. A simple classical choice for the stored energy is $W \stackrel{\text{def}}{=} \rho w = \frac{1}{2} (\boldsymbol{\varepsilon} - \boldsymbol{\beta}) : \mathbb{E} : (\boldsymbol{\varepsilon} - \boldsymbol{\beta}) + \rho \mathcal{C} \theta$, where $\boldsymbol{\varepsilon}$ denotes the infinitesimal strain, $\boldsymbol{\beta}$ the inelastic (eigen-) strains, such as thermal or plastic strains, and \mathcal{C} denotes the heat capacity per unit mass. To a first approximation the thermo-mechanical constitutive relationship can be written as $\boldsymbol{\varepsilon}_{\theta} = \gamma \cdot (\theta - \theta_0) \mathbf{1}$, $\boldsymbol{\sigma} = \mathbb{E} : (\boldsymbol{\varepsilon} - \boldsymbol{\varepsilon}_{\theta})$, where $\boldsymbol{\sigma}$ is the Cauchy stress, γ is the coefficient (matrix in the anisotropic case) of thermal expansion, and θ_0 is the temperature at which no thermal strains occur. Quantities such as plastic strains and other eigenstrains, for example due to phase transformations, are not considered in this work, although their treatment can be found in the Habilitation thesis of Zohdi [14]. However, to keep the notation somewhat general, the symbol $\boldsymbol{\beta}$ is still used for the sum of all inelastic strains, even though later in the simulations only $\boldsymbol{\beta} = \boldsymbol{\varepsilon}_{\theta}$ is considered. This leaves, with $\boldsymbol{\sigma} : \nabla \dot{\mathbf{u}} = (\mathbb{E} : (\boldsymbol{\varepsilon} - \boldsymbol{\beta})) : \dot{\boldsymbol{\varepsilon}}$, the following balance of energy:

$$-\nabla \cdot \mathbf{q} = \rho \mathcal{C} \dot{\theta} + \rho \dot{\mathcal{C}} \theta + \frac{1}{2} (\boldsymbol{\varepsilon} - \boldsymbol{\beta}) : \dot{\mathbb{E}} : (\boldsymbol{\varepsilon} - \boldsymbol{\beta}) - \dot{\boldsymbol{\beta}} : \mathbb{E} : (\boldsymbol{\varepsilon} - \boldsymbol{\beta}) - \rho z \quad (3)$$

where $\dot{\rho} \approx 0$, since the strains are assumed to be small.

2.4. A phenomenological damage model

As mentioned in the introduction, knowledge of the deterioration of the material properties, such as \mathbb{E} , over time is of primary interest to a structural analyst. Typically, subcontinuum failure mechanisms, which are the root cause for such continuum-scale material changes are virtually impossible to directly incorporate in practical continuum mesoscale and macroscale simulations. Therefore, a widely used approach to describe the deterioration of material responses is to employ phenomenologically based damage parameters governed by evolution laws. These are applied directly on the continuum level in order to represent the observed deteriorating responses of material samples with increasing time. There are a variety of such approaches, generally referred to as continuum damage mechanics models. For an overview of the field see References [15–17]. In this work a relatively standard evolution law form is used, namely $\dot{\mathbb{E}} = g\mathbb{E}$, where $g = g(c, \theta, \boldsymbol{\sigma})$ is a scalar damage function. Specifically, the description is of the form $\dot{\alpha}\mathbb{E}_0 = g\alpha\mathbb{E}_0$ which implies that, $\dot{\alpha} = g\alpha$, where \mathbb{E}_0 is the original undamaged material, and where, at each point in the material, the scalar parameter function obeys¹

$$\begin{aligned}
 \dot{\alpha} &= \underbrace{(A_1 c + A_2 \frac{\|\boldsymbol{\sigma}\| - \sigma_{\text{crit}}}{\sigma_{\text{crit}}})}_g \alpha \\
 \text{IF } c < c_{\text{crit}} \text{ THEN } A_1 &= 0 \\
 \text{IF } c \geq c_{\text{crit}} \text{ THEN } A_1 &= A_1^* \\
 \text{IF } \|\boldsymbol{\sigma}\| \stackrel{\text{def}}{=} \sqrt{\boldsymbol{\sigma} : \boldsymbol{\sigma}} < \sigma_{\text{crit}} \text{ THEN } A_2 &= 0 \\
 \text{IF } \|\boldsymbol{\sigma}\| \stackrel{\text{def}}{=} \sqrt{\boldsymbol{\sigma} : \boldsymbol{\sigma}} \geq \sigma_{\text{crit}} \text{ THEN } A_2 &= A_2^*
 \end{aligned} \tag{4}$$

where $A_1^* \leq 0$ and $A_2^* \leq 0$ are spatially variable material parameters, and where $\alpha(t=0) = 1$. For any later time t , $0 < \alpha \leq 1$. If $\alpha = 1$ at a point, then material is undamaged, and as $\alpha \rightarrow 0$ the material becomes completely damaged. The scalar function α takes on different values throughout the body, dictated by the evolution law. The spatially variable term σ_{crit} , a material constant, is a critical level of stress, while the spatially variable term c_{crit} , also a material constant, is a critical threshold value of the diffusing species for the inception of chemical damage. The $A_1 c$ term accounts for chemical damage, while the $A_2(\|\boldsymbol{\sigma}\| - \sigma_{\text{crit}})/\sigma_{\text{crit}}$ accounts for mechanical damage, for example due to high thermally-induced stresses, and can be thought of as an ‘overstress’ evolution function for microdamage. For further details on this relatively standard damage mechanics formulation, the reader is referred to References [15–17].

Remark 1. The chemical production of energy at a point is phenomenologically modeled as being related to the change in the material’s properties, $\rho z = \zeta \|\dot{\mathbb{E}}\| \stackrel{\text{def}}{=} \hat{\zeta} |\dot{\alpha}|$, where $\hat{\zeta}$ is a spatially variable material constant. The parameter $\hat{\zeta}$ is negative for exothermic reactions and positive for endothermic reactions.

¹ The parameter α is sometimes known as the ‘continuity’ parameter [15].

Remark 2. Clearly, further evolution laws can be written for other material property changes, such as \mathbb{D} , \mathcal{C} , etc. However, in order to keep the upcoming analysis relatively simple, only changes in \mathbb{E} are presently considered.

3. A RECURSIVE FIXED-POINT STAGGERING STRATEGY

The analysis now turns to the primary concern of this work, namely the development of an adaptive recursive staggering strategy for the solution of a set of multifield coupled equations, such as those described in the previous section. As mentioned in the introduction, since the finite element meshes need to be extremely fine to capture the material microstructure, in order to reduce the computational effort, it is advantageous to use as large time step sizes as possible, while maintaining numerical accuracy.

3.1. The procedure

Consider the following weak forms for the field equations derived in the previous sections, where the coupling terms have been brought to the right-hand side:

<p><i>Mass balance of diffusing species</i></p> <p>Find $c \in H^1(\Omega)$, $c _{\Gamma_c} = C$, such that, $\forall v \in H^1(\Omega)$, $v _{\Gamma_c} = 0$</p> $\int_{\Omega} \nabla v \cdot \mathbb{D}_0 \mathbf{e}^{-U/R\theta} \cdot \nabla c \, d\Omega = - \int_{\Omega} v \dot{c} \, d\Omega - \int_{\Omega} v \tau^0 \mathbf{e}^{-Q/R\theta} c \, d\Omega + \int_{\Gamma_g} v \mathbf{G} \cdot \mathbf{n} \, dA$ <p><i>Energy balance</i></p> <p>Find $\theta \in H^1(\Omega)$, $\theta _{\Gamma_\theta} = \Theta$, such that $\forall v \in H^1(\Omega)$, $v _{\Gamma_\theta} = 0$</p> $\begin{aligned} \int_{\Omega} \nabla v \cdot \mathbb{K} \cdot \nabla \theta \, d\Omega = & - \int_{\Omega} v \frac{1}{2} (\boldsymbol{\varepsilon} - \boldsymbol{\beta}) : \dot{\mathbb{E}} : (\boldsymbol{\varepsilon} - \boldsymbol{\beta}) \, d\Omega - \int_{\Omega} v \rho \dot{\mathcal{C}} \theta \, d\Omega \\ & - \int_{\Omega} v \rho \dot{\mathcal{C}} \theta \, d\Omega + \int_{\Omega} v \dot{\boldsymbol{\beta}} : \mathbb{E} : (\boldsymbol{\varepsilon} - \boldsymbol{\beta}) \, d\Omega \\ & + \int_{\Omega} v \rho z \, d\Omega + \int_{\Gamma_q} v \mathbf{q} \cdot \mathbf{n} \, dA \end{aligned}$ <p><i>Momentum balance</i></p> <p>Find $\mathbf{u} \in \mathbf{H}^1(\Omega)$, $\mathbf{u} _{\Gamma_u} = \mathbf{d}$, such that $\forall \mathbf{v} \in \mathbf{H}^1(\Omega)$, $\mathbf{v} _{\Gamma_u} = \mathbf{0}$</p> $\int_{\Omega} \nabla \mathbf{v} : \mathbb{E} : \nabla \mathbf{u} \, d\Omega = \int_{\Gamma_t} \mathbf{t} \cdot \mathbf{v} \, dA + \int_{\Omega} \nabla \mathbf{v} : \mathbb{E} : \boldsymbol{\beta} \, d\Omega + \int_{\Omega} \mathbf{v} \cdot \rho \mathbf{b} \, d\Omega$	(5)
--	-----

For all time dependent variables, backward Euler time discretization is employed. For example for the diffusive species, the approximation is derived from a Taylor's series expansion about time

$$t^{L+1}, c^L = c^{L+1} - \frac{\partial c}{\partial t} \Big|_{t_{L+1}} (\Delta t) + \frac{1}{2} \frac{\partial^2 c}{\partial t^2} \Big|_{t_{L+1}} (\Delta t)^2 - \frac{1}{6} \frac{\partial^3 c}{\partial t^3} \Big|_{t_{L+1}} (\Delta t)^3 \dots$$

to give

$$\frac{\partial c}{\partial t} \Big|_{t_{L+1}} = \frac{c^{L+1} - c^L}{\Delta t} + \mathcal{O}(\Delta t)$$

The following algorithm drives the staggering process within a time step:²

(★) At a time step (L): start an internal iteration $I = 0$

(★★) *Mass balance of diffusing species*

Find $c^{L+1, I+1} \in H^1(\Omega)$, $c^{L+1, I+1}|_{\Gamma_c} = C^{L+1}$, such that $\forall v \in H^1(\Omega)$, $v|_{\Gamma_c} = 0$

$$\int_{\Omega} \nabla v \cdot \mathbb{D}_0^{L+1, I} e^{-U^{L+1, I}/R\theta^{L+1, I}} \cdot \nabla c^{L+1, I+1} \, d\Omega + \frac{1}{\Delta t} \int_{\Omega} v c^{L+1, I+1} \, d\Omega$$

$$+ \int_{\Omega} v \tau^0 e^{-Q^{L+1, I}/R\theta^{L+1, I}} c^{L+1, I+1} \, d\Omega = \frac{1}{\Delta t} \int_{\Omega} v c^L \, d\Omega + \int_{\Gamma_G} v \mathbf{G}^{L+1} \cdot \mathbf{n} \, dA$$

Reactions: $\alpha^{L+1, I+1} = g(c^{L+1, I+1}, \theta^{L+1, I}, \sigma^{L+1, I}) \alpha^{L+1, I+1} \Rightarrow \alpha^{L+1, I+1} = \alpha^L e^{g\Delta t}$

Heat generation: $(\rho z)^{L+1, I+1} = \hat{c} \alpha^{L+1, I+1}$

Energy equation: $(\beta^{L+1, I} \stackrel{\text{def}}{=} \gamma^{L+1, I+1} \cdot \Delta \theta^{L+1, I} \mathbf{1})$

Find $\theta^{L+1, I+1} \in H^1(\Omega)$, $\theta^{L+1, I+1}|_{\Gamma_\theta} = \Theta^{L+1}$, such that $\forall v \in H^1(\Omega)$, $v|_{\Gamma_\theta} = 0$

$$\int_{\Omega} \nabla v \cdot \mathbb{K}^{L+1, I+1} \cdot \nabla \theta^{L+1, I+1} \, d\Omega + \frac{1}{\Delta t} \int_{\Omega} v \rho \mathcal{C}^{L+1, I+1} \theta^{L+1, I+1} \, d\Omega$$

$$= \frac{1}{\Delta t} \int_{\Omega} v \rho \mathcal{C}^{L+1, I+1} \theta^L \, d\Omega + \int_{\Gamma_q} v \mathbf{q}^{L+1} \cdot \mathbf{n} \, dA - \int_{\Omega} v \rho \mathcal{C}^{L+1, I+1} \theta^{L+1, I+1} \, d\Omega$$

$$- \int_{\Omega} v \frac{1}{2} (\boldsymbol{\varepsilon}^{L+1, I} - \boldsymbol{\beta}^{L+1, I}) : \mathbb{E}^{L+1, I+1} : (\boldsymbol{\varepsilon}^{L+1, I} - \boldsymbol{\beta}^{L+1, I}) \, d\Omega$$

$$+ \int_{\Omega} (\rho z)^{L+1, I+1} v \, d\Omega + \int_{\Omega} v \boldsymbol{\beta}^{L+1, I} : \mathbb{E}^{L+1, I+1} : (\boldsymbol{\varepsilon}^{L+1, I} - \boldsymbol{\beta}^{L+1, I}) \, d\Omega$$

² Inertia (acceleration) terms are neglected. Also, Fourier's law of heat conduction is used. In addition, only for purposes of general algorithmic illustration, material parameters other than \mathbb{E} , such as \mathbb{D}_0 , \mathbb{K} , etc., are shown to change in Box 6.

<p><i>Balance of momentum:</i> ($\boldsymbol{\beta}^{L+1,I+1} \stackrel{\text{def}}{=} \boldsymbol{\gamma}^{L+1,I+1} \cdot \Delta \theta^{L+1,I+1} \mathbf{1}$)</p> <p>Find $\mathbf{u}^{L+1,I+1} \in \mathbf{H}^1(\Omega)$, $\mathbf{u}^{L+1,I+1} _{\Gamma_u} = \mathbf{d}^{L+1}$, such that $\forall \mathbf{v} \in \mathbf{H}^1(\Omega)$, $\mathbf{v} _{\Gamma_u} = \mathbf{0}$</p> $\int_{\Omega} \nabla \mathbf{v} : \mathbb{E}^{L+1,I+1} : \nabla \mathbf{u}^{L+1,I+1} \, d\Omega = \int_{\Gamma_t} \mathbf{t}^{L+1} \cdot \mathbf{v} \, dA + \int_{\Omega} \rho \mathbf{b}^{L+1} \cdot \mathbf{v} \, d\Omega$ $+ \int_{\Omega} \nabla \mathbf{v} : \mathbb{E}^{L+1,I+1} : \boldsymbol{\beta}^{L+1,I+1} \, d\Omega$ <p><i>Check for convergence:</i></p> $\frac{\ \alpha^{L+1,I+1} - \alpha^{L+1,I}\ _{L^1(\Omega)}}{\ \alpha^{L+1,I+1}\ _{L^1(\Omega)}} \leq \text{TOL}_{\alpha}, \quad \frac{\ \theta^{L+1,I+1} - \theta^{L+1,I}\ _{L^1(\Omega)}}{\ \theta^{L+1,I+1}\ _{L^1(\Omega)}} \leq \text{TOL}_{\theta}$ $\frac{\ \boldsymbol{\sigma}^{L+1,I+1} - \boldsymbol{\sigma}^{L+1,I}\ _{L^1(\Omega)}}{\ \boldsymbol{\sigma}^{L+1,I+1}\ _{L^1(\Omega)}} \leq \text{TOL}_{\sigma}, \quad \frac{\ c^{L+1,I+1} - c^{L+1,I}\ _{L^1(\Omega)}}{\ c^{L+1,I+1}\ _{L^1(\Omega)}} \leq \text{TOL}_c$ <p>IF tolerances not met THEN $I = I + 1$, GO TO ($\star\star$)</p> <p><i>Increment time:</i> $L = L + 1$, update all variables, GO TO (\star).</p>	(6)
--	-----

Remark 1. Writing the system of equations in this form produces three algebraic systems which are symmetric and positive definite. Therefore, standard fast iterative algebraic system solvers, such as the widely used preconditioned Conjugate Gradient Method, can be used. For details see Reference [18]. *It is crucial to use such iterative solvers, since any previous solution, from a previous time step or staggered iteration can be used as the first guess in the solution procedure.* Therefore, after the first time step, the computational solution time is extremely short. Furthermore, in the event that one field is insensitive, i.e. slowly varying during a time interval, the iterative solver will only need one or two iterations to update the solution, thus sparing a number of needless iterative operations.

Remark 2. Within a given time step, if the staggering scheme converges, it is to a monolithic scheme solution. The term ‘monolithic’ is used to denote the full coupled discrete system of equations. A monolithic solution procedure for this multifield system would be quite involved, since it would require a linearization of the equations, which is extremely difficult due to the equation coupling. Furthermore, a complete linearization would result in an indefinite non-symmetric system of equations, where, for example, a standard preconditioned Conjugate Gradient Method could not be used. *The form of staggering scheme presented here avoids both such problems.*

Remark 3. If the recursive strategy does not converge within a prespecified number of staggered iterations, the time step at stage L is adaptively scaled and the recursive staggering procedure is repeated. The details of this scaling process are discussed in the next section.

3.2. Recursive solution properties and adaptive time step error control

Consider a general system of coupled partial differential equations given by $\mathcal{A}(\mathbf{w}) = \mathcal{F}$, where \mathbf{w} is a solution, and where it is assumed that the operator, \mathcal{A} , is invertible. One desires that the sequence of iterated solutions, \mathbf{w}^I , $I = 1, 2, \dots$, converge to $\mathcal{A}^{-1}(\mathcal{F})$ as $I \rightarrow \infty$. If \mathbf{w}^I is a function of $\mathcal{A}, \mathcal{F}, \mathbf{w}^1, \dots, \mathbf{w}^{I-K}$ one says that K is the order of iteration. It is assumed that the I th iterate can be represented by some arbitrary function $\mathbf{w}^I = \mathcal{F}^I(\mathcal{A}, \mathcal{F}, \mathbf{w}^{I-1})$. One makes the following split $\mathbf{w}^I = \mathcal{G}^I(\mathbf{w}^{I-1}) + \mathbf{r}^I$. For this method to be useful the exact solution should be reproduced. In other words, when $\mathbf{w} = \mathcal{A}^{-1}(\mathcal{F})$, then $\mathbf{w} = \mathcal{A}^{-1}(\mathcal{F}) = \mathcal{G}^I(\mathcal{A}^{-1}(\mathcal{F})) + \mathbf{r}^I$. Therefore, one has the following consistency condition $\mathbf{r}^I = \mathcal{A}^{-1}(\mathcal{F}) - \mathcal{G}^I(\mathcal{A}^{-1}(\mathcal{F}))$, and as a consequence, $\mathbf{w}^I = \mathcal{G}^I(\mathbf{w}^{I-1}) + \mathcal{A}^{-1}(\mathcal{F}) - \mathcal{G}^I(\mathcal{A}^{-1}(\mathcal{F}))$. Convergence of the iteration can be studied by defining the error vector:

$$\begin{aligned} \mathbf{e}^I &= \mathbf{w}^I - \mathbf{w} \\ &= \mathbf{w}^I - \mathcal{A}^{-1}(\mathcal{F}) \\ &= \mathcal{G}^I(\mathbf{w}^{I-1}) + \mathcal{A}^{-1}(\mathcal{F}) - \mathcal{G}^I(\mathcal{A}^{-1}(\mathcal{F})) - \mathcal{A}^{-1}(\mathcal{F}) \\ &= \mathcal{G}^I(\mathbf{w}^{I-1}) - \mathcal{G}^I(\mathcal{A}^{-1}(\mathcal{F})) \end{aligned} \quad (7)$$

One sees that, if \mathcal{G}^I is linear and invertible, the above reduces to $\mathbf{e}^I = \mathcal{G}^I(\mathbf{w}^{I-1} - \mathcal{A}^{-1}(\mathcal{F})) = \mathcal{G}^I(\mathbf{e}^{I-1})$. Therefore, if the spectral radius of \mathcal{G}^I , i.e. the magnitude of its largest eigenvalue, is less than unity for each iteration I , then $\mathbf{e}^I \rightarrow \mathbf{0}$ for any arbitrary starting solution $\mathbf{w}^{I=0}$ as $I \rightarrow \infty$. *This sufficient, but not necessary, condition for convergence will be exploited in this work.*

3.3. Time step dependency of the coupled spectral radius

For the class of coupled systems considered in this work the coupled operator's spectral radius is directly dependent on the time step discretization Δt . As an example, consider the following simple coupled system:

$$\boxed{\begin{aligned} a\dot{w}_1 &= w_2 \\ b\dot{w}_2 &= w_1 \end{aligned}} \quad (8)$$

When discretized in time, for example with a backward Euler scheme, one obtains the following coupled system:

$$\begin{bmatrix} 1 & -\frac{\Delta t}{a} \\ -\frac{\Delta t}{b} & 1 \end{bmatrix} \begin{bmatrix} w_1^{L+1, I+1} \\ w_2^{L+1, I+1} \end{bmatrix} = \begin{bmatrix} w_1^L \\ w_2^L \end{bmatrix} \quad (9)$$

where L is a time increment counter, and I is an internal staggering iteration counter. For a recursive staggering scheme of Jacobi-type, considered here only for algebraic simplicity,³ one has

$$\begin{bmatrix} 1 & 0 \\ 0 & 1 \end{bmatrix} \begin{bmatrix} w_1^{L+1,I+1} \\ w_2^{L+1,I+1} \end{bmatrix} = \begin{bmatrix} w_1^L \\ w_2^L \end{bmatrix} + \begin{bmatrix} \frac{\Delta t}{a} w_2^{L+1,I} \\ \frac{\Delta t}{b} w_1^{L+1,I} \end{bmatrix} \quad (10)$$

Rewriting this in terms of the \mathcal{G} -form yields

$$\underbrace{\begin{bmatrix} 0 & \frac{\Delta t}{a} \\ \frac{\Delta t}{b} & 0 \end{bmatrix}}_{\mathcal{G}} \underbrace{\begin{bmatrix} w_1^{L+1,I} \\ w_2^{L+1,I} \end{bmatrix}}_{\mathbf{w}^I} = \underbrace{\begin{bmatrix} w_1^{L+1,I+1} \\ w_2^{L+1,I+1} \end{bmatrix}}_{\mathbf{w}^{I+1}} - \underbrace{\begin{bmatrix} w_1^L \\ w_2^L \end{bmatrix}}_r \quad (11)$$

The eigenvalues of \mathcal{G} are $\mathcal{E}\mathcal{I}\mathcal{G}(\mathcal{G}) = \pm\sqrt{(\Delta t)^2/ab}$. One sees that the convergence of the staggering scheme is directly related (linearly in this case) to the size of the time step. The solution to the example is

$$\begin{aligned} w_1^{L+1} &= \frac{\frac{\Delta t}{a} w_2^L + w_1^L}{1 - \frac{(\Delta t)^2}{ab}} = \underbrace{w_1^L + \frac{w_2^L \Delta t}{a}}_{\text{first staggered iteration}} + \underbrace{\frac{w_1^L (\Delta t)^2}{ab}}_{\text{second staggered iteration}} + \dots \\ w_2^{L+1} &= \frac{\frac{\Delta t}{b} w_1^L + w_2^L}{1 - \frac{(\Delta t)^2}{ab}} = \underbrace{w_2^L + \frac{w_1^L \Delta t}{b}}_{\text{first staggered iteration}} + \underbrace{\frac{w_2^L (\Delta t)^2}{ab}}_{\text{second staggered iteration}} + \dots \end{aligned} \quad (12)$$

An important observation is that the time step induced restriction for convergence matches the radius of analyticity of a Taylor series expansion of the solution around the previous time increment solution. As is well known, a Taylor series converges in a ball of radius from the point of expansion to the nearest singularity. In other words, the limiting step size is given by setting the denominator to zero, $1 - (\Delta t)^2/ab = 0$, which is in agreement with the condition derived from the analysis of the eigenvalues of \mathcal{G} . Clearly, the convergence,

³ A Gauss-Seidel-type approach would involve using the most current iterate. This is used in the three-dimensional simulations.

as well as the convergence rate, of the recursive scheme depends on the time step size. Furthermore, if the recursive process is *not employed*, as in standard staggering schemes, the error, which is of first order in Δt , can accumulate relatively rapidly. Therefore, if one wishes to reduce computational effort by employing larger time steps, the recursive solution technique is essential. Obviously there is a tradeoff of whether one should use many small time steps, which will require less internal iterations to reduce the staggering error, or less larger time steps, which require relatively more internal iterations to reduce the staggering error. Therefore, the objective of the next section is to develop a strategy to adaptively adjust the choice of time step size, to minimize the computational effort, while delivering approximate solutions below a prespecified error tolerance. The number of times the multifield system is solved, as opposed to time steps, is taken as the measure of computational effort, since within a time step, many multifield system re-solves can take place.

3.4. Temporal control of the spectral radius

Motivated by the previous analysis, one approximates the spectral radius of \mathcal{G} by $\max \mathcal{E} \mathcal{I} \mathcal{G}(\mathcal{G}) \approx S \Delta t$, where one expects the error within an iteration to behave according to $(S \Delta t)^I e_0 = e_I$, $I = 1, 2, \dots$, where e_0 is the initial error and S (dependent upon \mathcal{G} , I and implicitly on Δt) is a function intrinsic to the system. *Our target or ideal condition is to meet an error tolerance in a given number of iterations, not more, and not less.* One writes this in the following approximate form, $(S \Delta t_{\text{tol}})^{I_d} e_0 = e_{\text{tol}}$, where I_d is the number of desired iterations. Therefore, if the error tolerance is not met in the desired number of iterations, the spectral radius is too large. Accordingly, one can solve for a new smaller step size, under the assumption that S is constant,

$$\Delta t_{\text{tol}} = \Delta t \left(\frac{(e_{\text{tol}}/e_0)^{1/I_d}}{(e_I/e_0)^{1/I}} \right) \quad (13)$$

The assumption that S is constant is not overly severe, since the time steps are to be recursively refined and unrefined. Clearly, the expression in Box 13 is to be used for time step enlargement, if convergence is met in less than I_d iterations. One sees that if $e_{I_d} > e_{\text{tol}}$ when $I = I_d$, then the expression in Box 13 collapses to a ratio of the error tolerance to the achieved level of iterative error after I_d iterations,

$$\Delta t_{\text{tol}} = \Delta t \left(\frac{e_{\text{tol}}}{e_{I_d}} \right)^{1/I_d} \quad (14)$$

and thus the step size will be reduced. An adaptive time stepping strategy readily follows:

At a time step (L)

$$r_\alpha \stackrel{\text{def}}{=} \frac{e_\alpha}{\text{TOL}_\alpha} \quad r_\theta \stackrel{\text{def}}{=} \frac{e_\theta}{\text{TOL}_\theta} \quad r_c \stackrel{\text{def}}{=} \frac{e_c}{\text{TOL}_c} \quad r_\sigma \stackrel{\text{def}}{=} \frac{e_\sigma}{\text{TOL}_\sigma}$$

$$e_\alpha \stackrel{\text{def}}{=} \frac{\|\alpha^{L+1,I} - \alpha^{L+1,I-1}\|_{L^1(\Omega)}}{\|\alpha^{L+1,I}\|_{L^1(\Omega)}} \quad e_\theta \stackrel{\text{def}}{=} \frac{\|\theta^{L+1,I} - \theta^{L+1,I-1}\|_{L^1(\Omega)}}{\|\theta^{L+1,I}\|_{L^1(\Omega)}}$$

$$e_\sigma \stackrel{\text{def}}{=} \frac{\|\sigma^{L+1,I} - \sigma^{L+1,I-1}\|_{L^1(\Omega)}}{\|\sigma^{L+1,I}\|_{L^1(\Omega)}} \quad e_c \stackrel{\text{def}}{=} \frac{\|c^{L+1,I} - c^{L+1,I-1}\|_{L^1(\Omega)}}{\|c^{L+1,I}\|_{L^1(\Omega)}}$$

From $\max(r_\alpha, r_\theta, r_\sigma, r_c) \Rightarrow$ select corresponding $e \stackrel{\text{def}}{=} e^*$

IF tolerance not met THEN: ($e_{\text{tol}}^* < e_I^*$, $I = I_d$) (15)

$$t = t - \Delta t \quad \Delta t_{\text{tol}} = \Delta t \left(\frac{e_{\text{tol}}^*}{e_I^*} \right)^{1/I_d} \quad t = t + \Delta t_{\text{tol}}$$

Restart computations at time step (L)

IF tolerance met THEN: ($e_{\text{tol}}^* \geq e_I^*$, $I \leq I_d$)

$$\Delta t_{\text{tol}} = \Delta t \left(\frac{(e_{\text{tol}}^*/e_0^*)^{1/I_d}}{(e_I^*/e_0^*)^{1/I}} \right) \quad t = t + \Delta t_{\text{tol}}$$

Start computations at time step ($L + 1$)

Remark 1. Although not employed in this work, convergence of the staggering scheme may be further enhanced by application of overrelaxation methods in a similar manner as used in classical iterative algebraic system solving ([25–28]).

Remark 2. As mentioned, an alternative approach is to attempt to solve the entire system simultaneously (monolithically). This would involve the use of a Newton-type scheme, which can also be considered as a type of fixed-point iteration. In this case one can write the following: $\mathbf{w}^I - \mathbf{w} = (\mathcal{G}^I(\mathbf{w}^{I-1}) + \mathbf{r}^I) - (\mathcal{G}^I(\mathbf{w}) + \mathbf{r}^I)$. Furthermore, one has from a generalized Taylor’s series expansion $\mathcal{G}^I(\mathbf{w}) = \mathcal{G}^I(\mathbf{w}^{I-1}) + (\nabla_{\mathbf{w}} \mathcal{G}^I)|_{\mathbf{w}^{I-1}}(\mathbf{w} - \mathbf{w}^{I-1}) + \mathcal{O}(\|\mathbf{w}^{I-1} - \mathbf{w}\|^2)$, and thus

$$\begin{aligned} \mathbf{w}^I - \mathbf{w} &= \mathcal{G}^I(\mathbf{w}^{I-1}) - (\mathcal{G}^I(\mathbf{w}^{I-1}) + (\nabla_{\mathbf{w}} \mathcal{G}^I)|_{\mathbf{w}^{I-1}}(\mathbf{w} - \mathbf{w}^{I-1}) + \mathcal{O}(\|\mathbf{w}^{I-1} - \mathbf{w}\|^2)) \\ &= -(\nabla_{\mathbf{w}} \mathcal{G}^I)|_{\mathbf{w}^{I-1}}(\mathbf{w}^{I-1} - \mathbf{w}) - \mathcal{O}(\|\mathbf{w}^{I-1} - \mathbf{w}\|^2) \end{aligned} \tag{16}$$

Therefore, if the spectral radius of $(\nabla_{\mathbf{w}} \mathcal{G}^{I+1})|_{\mathbf{w}^I}$ is less than one, then $\mathbf{e}^I \rightarrow \mathbf{0}$ for an arbitrary starting solution $\mathbf{w}^{I=0}$ as $I \rightarrow \infty$. As in the linear- \mathcal{G} case this condition is a sufficient, but not

necessary, condition for convergence. Newton's method is covered as a special case of this general analysis. To see this, consider that Newton updating can be written as

$$\mathbf{w}^I = \underbrace{\mathbf{w}^{I-1}}_{\mathbf{r}^I} - \underbrace{(\mathcal{A}^{\text{TAN},I-1})^{-1} \mathcal{R}(\mathbf{w}^{I-1})}_{\mathcal{G}(\mathbf{w}^{I-1})} \quad (17)$$

where $\mathcal{R} \stackrel{\text{def}}{=} \mathcal{A}(\mathbf{w}) - \mathcal{F}$ is the residual, and $\mathcal{A}^{\text{TAN},I} = (\nabla_{\mathbf{w}} \mathcal{A}(\mathbf{w}))|_{\mathbf{w}^I}$ is the tangent. Therefore, in the fixed-point form one has the operator $\mathcal{G}(\mathbf{w}) = \mathbf{w} - (\mathcal{A}^{\text{TAN}})^{-1} \mathcal{R}(\mathbf{w})$. The gradient is

$$\begin{aligned} \nabla_{\mathbf{w}} \mathcal{G}(\mathbf{w}) &= \mathbf{I} + (\mathcal{A}^{\text{TAN}})^{-2} (\mathcal{A}^{\text{TAN}})^{\text{TAN}} \mathcal{R}(\mathbf{w}) - (\mathcal{A}^{\text{TAN}})^{-1} \mathcal{A}^{\text{TAN}} \\ &= ((\mathcal{A}^{\text{TAN}})^{-2} (\mathcal{A}^{\text{TAN}})^{\text{TAN}} \mathcal{R}(\mathbf{w})) \end{aligned} \quad (18)$$

where $(\mathcal{A}^{\text{TAN}})^{\text{TAN}} \stackrel{\text{def}}{=} \nabla_{\mathbf{w}} (\nabla_{\mathbf{w}} \mathcal{A}(\mathbf{w}))$. Therefore, the convergence criteria is, $\forall I = 1, 2, \dots$,

$$|\mathcal{G} \mathcal{G}((\mathcal{A}^{\text{TAN},I})^{-2} (\mathcal{A}^{\text{TAN},I})^{\text{TAN},I} \mathcal{R}(\mathbf{w}^I))| < 1 \quad (19)$$

Therefore, one immediately sees a fundamental difficulty, due to the possibility of a zero, or near zero, tangent when employing a Newton's method to a system describing a weakening material. For example, consider a material law of the form $\boldsymbol{\sigma} = \alpha \mathbb{E} : \boldsymbol{\varepsilon}$, where $0 < \alpha \leq 1$ and $d\alpha \leq 0$, which possesses a tangent of the form $d\boldsymbol{\sigma} = d\alpha \mathbb{E} : \boldsymbol{\varepsilon} + \alpha \mathbb{E} : d\boldsymbol{\varepsilon} \stackrel{\text{def}}{=} \mathbb{E}^{\text{TAN}} : d\boldsymbol{\varepsilon}$. In this case, \mathbb{E}^{TAN} can lose positive definiteness when the change in α is sufficiently large, which in turn will lead to an indefinite-type system of algebraic equations. For early general work on fixed-point methods, the reader is referred to Perron [19] (1929), with subsequent results given by Ostrowski [20, 21], Ortega and Rockoff [22], Kitchen [23] and numerous others. For an overview see Reference [24].

Remark 3. The algorithm in Box 15 attempts to refine and unrefine the time steps to induce fixed-point type convergence of the recursive algorithm in Box 6 within a designated number of internal iterations. However, whenever one employs time discretization, one must contend with issues of stability. By stability one means that the errors made at one stage of the calculations do not cause increasingly large errors as the computations are continued, but will eventually damp out. For the implicit backward Euler type, there is an upper limit for the step size that can be used to retain computational stability, i.e. to avoid spurious oscillations. For the class of equations considered in this paper, the most sensitive part is the diffusion-reaction equation for autocatalytic cases. Some useful information can be extracted about stability limits from studying the uncoupled diffusion-reaction model in one dimension, $Dd^2c/dx^2 - \tau c = \dot{c}$. Discretizing this equation with the backward Euler scheme and assuming, for the moment, that D and τ are constants, then $Dd^2c/dx^2|_{L+1} - \tau c = (c^{L+1} - c^L)/(\Delta t)$ which implies

$$\frac{d^2c}{dx^2} \Big|_{L+1} - \frac{1}{D} \left(\frac{1}{\Delta t} + \tau \right) c^{L+1} = - \frac{c^L}{D\Delta t}$$

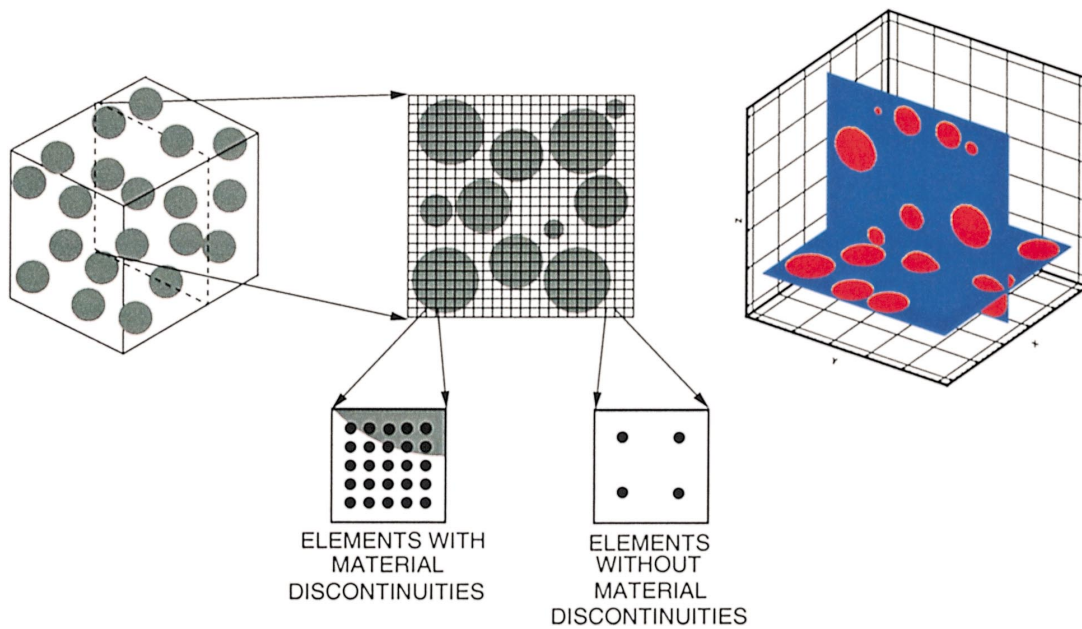


Plate 1. Left: A *cross-section* of the mesh density used in the numerical experiments. Approximately $9 \times 9 \times 9$ hexahedra per particle were used, as well as a '2/5' Gauss integration rule, i.e. a $2 \times 2 \times 2$ rule if there was no material discontinuity in the element, and a $5 \times 5 \times 5$ rule if there was a material discontinuity, in order to better capture the geometry within the element. Right: Mutually orthogonal cross-sections showing a dispersed 40 particle geometry used in the numerical simulations. The red color represents the particles and blue represents the matrix.

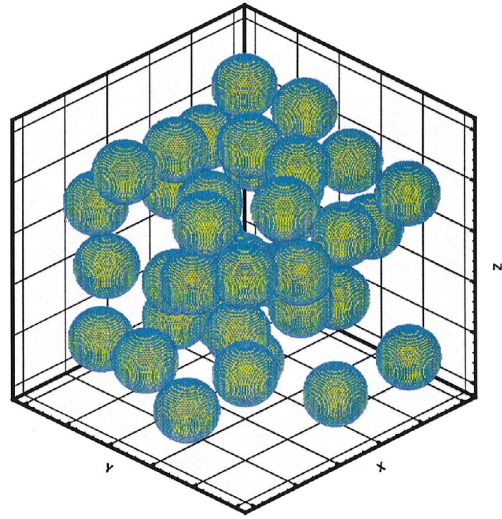
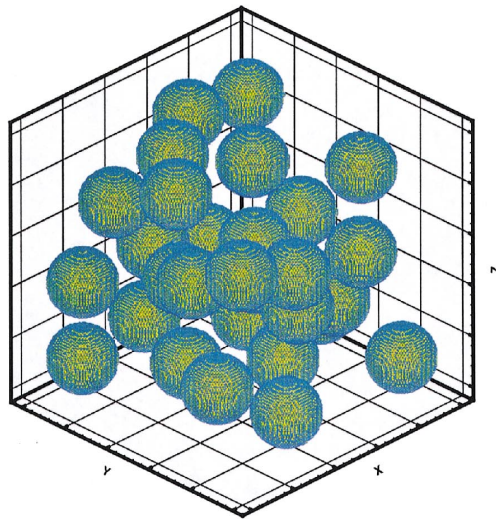
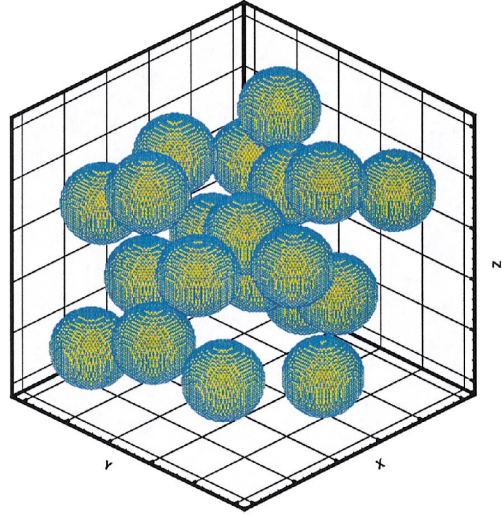
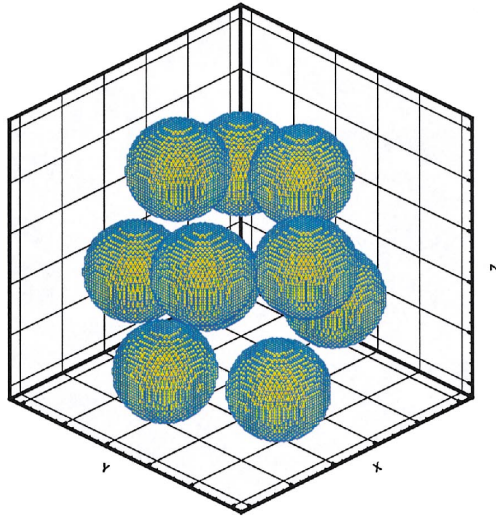


Plate 2. Numerical resolution of random microstructures consisting of 10, 20, 30 and 40 non-intersecting spheres, occupying approximately 22 per cent of the volume in a homogeneous matrix.

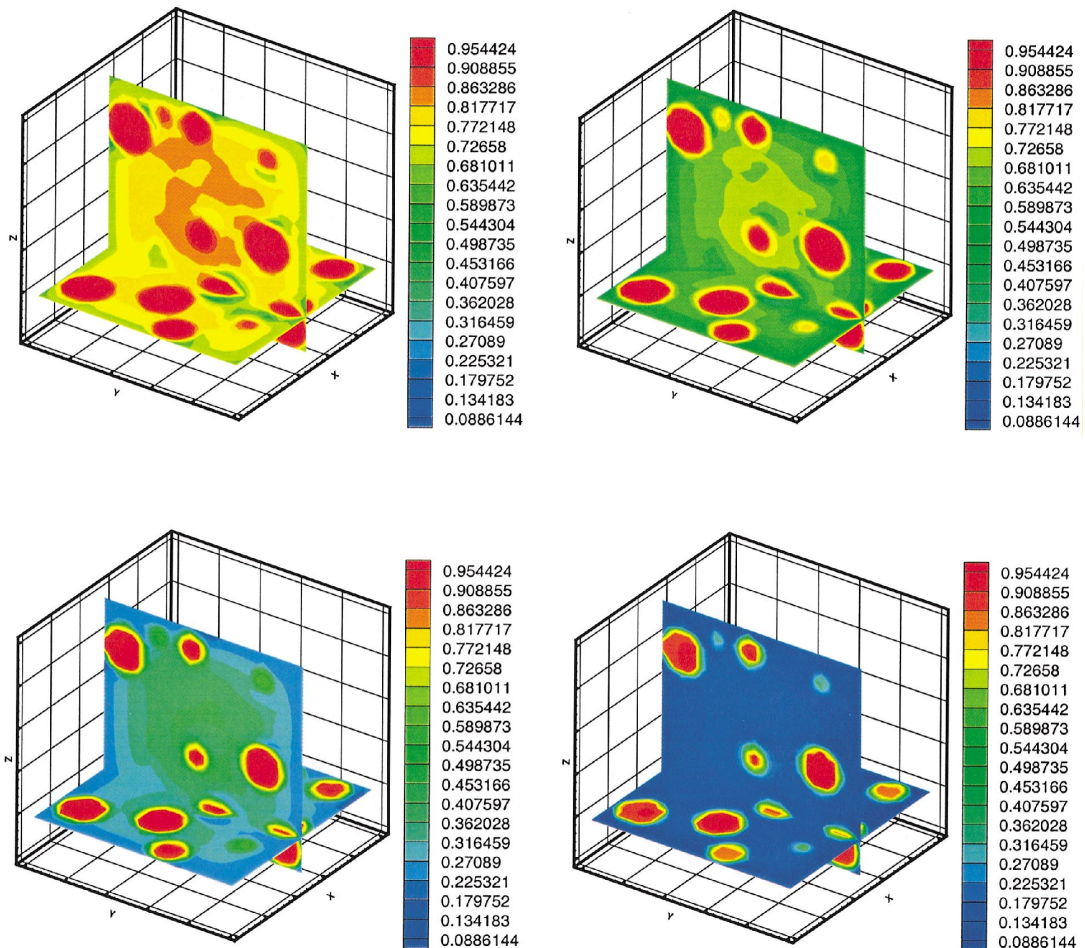


Plate 3. 40 Particle sample/autocatalytic regime: a value $\alpha=1$ represents a completely undamaged material, while a value of $\alpha=0$ represents a completely damaged material. Successive mutually orthogonal slices of the damage within the *three-dimensional* material sample after 15 000, 25 000, 50 000, and 100 000 s.

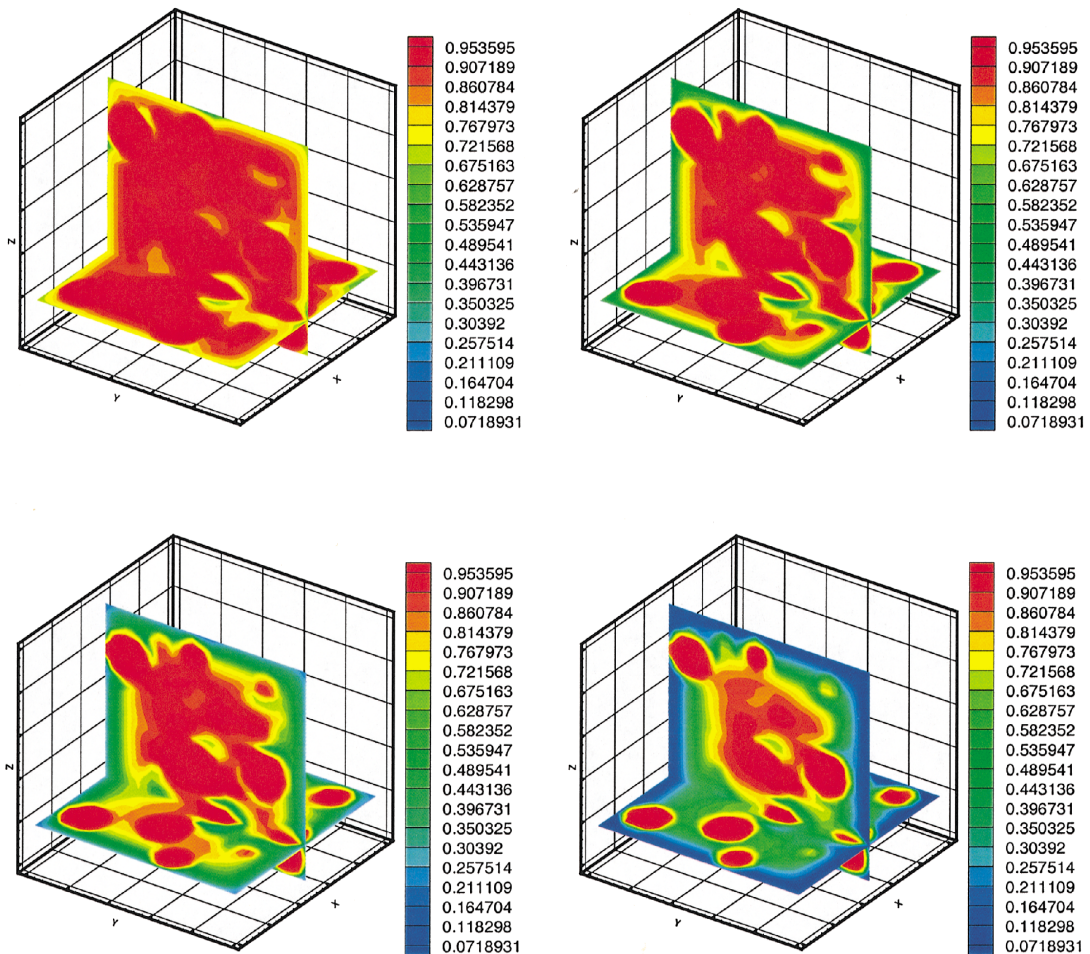


Plate 4. 40 Particle sample/non-autocatalytic regime: A value $\alpha=1$ represents a completely undamaged material, while a value of $\alpha=0$ represents a completely damaged material. Successive mutually orthogonal slices of the damage within the *three-dimensional* material sample after 15 000, 25 000, 50 000, and 100 000 s.

When $\tau < 0$, one observes that the system is of non-oscillatory type only for small Δt . If Δt becomes too large τ will dominate, and the system will exhibit spurious, *coarse time-step induced*, oscillations. Therefore, for the three-dimensional simulations to follow, for autocatalytic cases, $\Delta t = |(\tau^0)^{-1}|$ was used as a somewhat adhoc *upper limit* during adaptive time stepping. More comments on this point are made later in the presentation.

4. NUMERICAL EXAMPLES

Consistent with the structural engineering interests mentioned in the beginning of this work, the solution strategy was applied to samples of particulate materials. The macroscopic (structural scale) time dependent quantities of interest, generated by volumetric averaging the microscopic multifield solution, were (1) the mechanical response, $\langle \boldsymbol{\sigma} \rangle_{\Omega}$, (2) the average damage in the material, $\langle \alpha \rangle_{\Omega}$, (3) the average temperature, $\langle \theta \rangle_{\Omega}$, and (4) the average concentration $\langle c \rangle_{\Omega}$. For the tests, samples of material composed of a homogeneous matrix cube of dimensions $L \times L \times L$ containing N non-intersecting randomly dispersed spherical particles, of diameter d were considered (Plate 1). The amount of embedded particulate matter was specified by defining a subvolume size, $V \stackrel{\text{def}}{=} L \times L \times L/N$, where L was the length of the (cubical) sample, The ratio between the diameter and the subvolume was a control parameter defined by $\zeta \stackrel{\text{def}}{=} d/V^{1/3}$. For the numerical tests, a relatively high volume fraction was selected, approximately 22 per cent ($\zeta = 0.75$). In order to obtain statistically representative macroscopic responses, sample size enlargement tests, i.e. increasing the number of particles contained in the sample, holding the volume fraction constant, thus decreasing d/L , were performed. The test samples were as follows, where number of particles contained in a sample (of normalized size) was increased from 10, to 20 to 30 and finally to 40, while holding the volume fraction constant (Plate 2). Over the course of such tests the finite element meshes were repeatedly refined, and a mesh density of approximately $9 \times 9 \times 9$ trilinear hexahedra (approximately 800–1000 degrees of freedom (DOF) for the diffusion-reaction and energy balance equations, and between 2200 and 3000 DOF for the vector-valued balance of momentum) *per particle* was found to deliver mesh independent results. Therefore, for example for the 10 particle test, 8000 DOF were needed for the diffusion-reaction and energy balance equation, and 24000 DOF for the balance of momentum equation. For the other tests the degrees of freedom were, for 20 particles, 15 625 DOF/46 875 DOF, for 30 particles, 24 389 DOF/73 167 DOF and for 40 particles, 32 768 DOF/98 304 DOF. During the computations, a ‘2/5’ Gauss rule was used, whereby elements containing material discontinuities had increased Gauss rules ($5 \times 5 \times 5$) to enhance the resolution of the internal geometry, while elements with no material discontinuities had the nominal $2 \times 2 \times 2$ rule (Plate 1). The numerical resolution for each sample size’s microstructure is shown in Plate 2. Also, to increase the statistical representativeness of the sample enlargement testing process, 10 different samples, each possessing a different random particulate distribution, were tested at each size, and the results (ensemble) averaged. For more details about such numerical procedures, the reader is referred to References [29–34].

Simply to illustrate the solution algorithm, the boundary conditions for the multifield problem were

- CHEMICAL: $c|_{\partial\Omega} = C = 1$, $c(\mathbf{x}, t = 0) = 0$.
- THERMAL: $\theta|_{\partial\Omega} = \Theta = 0^\circ\text{C} = 273.15\text{ K}$, $\theta(\mathbf{x}, t = 0) = 0^\circ\text{C} = 273.15\text{ K}$.

Table I. Material properties used in the computational examples.

Material property	Matrix	Particles
<i>Mechanical</i>		
κ (GPa)	77.9	230.0
μ (GPa)	25.9	172.0
γ (1/K)	9.71×10^{-6}	8.92×10^{-6}
σ_{crit} (MPa)	120	3000
<i>Thermal</i>		
K (J/s m K)	237	148
ρ (kg/m ³)	2700.84	2330.28
C (J/kg K)	903	712
<i>Diffusive</i>		
D^0 (m/s ²)	1.0×10^{-6}	1.0×10^{-7}
$U_{\text{kN}} - \text{m/mole}$	142	300
τ^0 (1/s)	$\pm 1.0 \times 10^{-4}$	$\pm 1.0 \times 10^{-4}$
Q (kJ - m/mole)	142	300
<i>Damage evolution</i>		
A_1^* (m ³ /molecules s)	-2.665×10^{-5}	-1.219×10^{-6}
A_2^* (1/s)	-2.665×10^{-5}	-1.219×10^{-6}
$\hat{\zeta}$ (N m)	-200×10^9	-100×10^9
c_{crit} (molecules/m ³)	0.0	0.0

- MECHANICAL: $\mathbf{u}|_{\partial\Omega} = \mathcal{E} \cdot \mathbf{x}$, $\mathcal{E}_{ij} = 0.001$, $i, j = 1, 2, 3$, in other words

$$\begin{bmatrix} u_1|_{\partial\Omega} \\ u_2|_{\partial\Omega} \\ u_3|_{\partial\Omega} \end{bmatrix} = \underbrace{\begin{bmatrix} \mathcal{E}_{11} & \mathcal{E}_{12} & \mathcal{E}_{13} \\ \mathcal{E}_{12} & \mathcal{E}_{22} & \mathcal{E}_{23} \\ \mathcal{E}_{31} & \mathcal{E}_{32} & \mathcal{E}_{33} \end{bmatrix}}_{\mathcal{E}} \begin{bmatrix} x_1 \\ x_2 \\ x_3 \end{bmatrix} \quad (20)$$

where \mathbf{x} is a position vector to the boundary of the cube.

A simulation time of 100 000 s was selected, which is slightly over one day (86 400 s). Non-autocatalytic ($\tau^0 > 0$) and autocatalytic processes ($\tau^0 < 0$) were considered. The material parameters, *selected only for the purposes of numerical experiment*, are shown in Table I, and roughly correspond to a certain type of aluminum–boron composite, widely used for its lightweight, and relatively high strength. *For the purposes of numerical experiment only*, the damage rate parameters were chosen such that for a material point undergoing constant damage at unit concentration, with no stress, $\alpha(t = 86\,400) = 0.1 = e^{A_1^* t}$, which led to $A_1^* = -0.00002665$ (m³/molecules s). This rate was used for the matrix. For the particulate material, $\alpha(t = 86\,400) = 0.9 = e^{A_1^* t}$, which led to $A_1^* = -0.000001219$ (m³/molecules s). These values were also selected for the A_2^* rates as well. The deterioration rates of all material parameters other than \mathbb{E} , such as \mathcal{C} , \mathbb{K} , \mathbb{D} , etc., were set to zero, for lack of any supporting experimental data.

Typically, for a strongly coupled system, it is extremely difficult to determine the required time step size for numerical accuracy a priori. Therefore, for comparison purposes, standard staggering simulations were performed, i.e. without recursive solving or time step adaptivity. With the standard approach, successively smaller and smaller time steps were used until the numerical results stabilized, i.e. until they became invariant for further step size refinement. A time step size, Δt , of approximately 10 s was found to give time step invariant results. Such a time step size required approximately 10 000 multifield system solves. Essentially, the fine time step sizes were necessary in the beginning of the multifield process, which became 'overkill' as time progressed. To illustrate the possible benefits of the recursive adaptive algorithm developed, the adaptive-recursive procedure was started at a $\Delta t = 10$ s resolution. The algorithmic tolerance was set to $\max(e_x, e_\theta, e_\sigma, e_c) \leq 0.0001$, as defined in Box 15. The designated maximum number of internal iterations, I_d , was set to five. In order to smoothly refine and unrefine the time steps, the adjustments were bounded *between successive time steps* (L) to be $0.1 \leq \Delta t^{L+1}/\Delta t^L \leq 10$. It is remarked that for the autocatalytic case, the previously mentioned absolute time step limit for numerical stability, $|(\tau^0)^{-1}| = 10\,000$ s, was enforced. For the autocatalytic cases, larger time step limits were tested, with spurious oscillations occurring at roughly time step sizes of 15 000 s. For the non-autocatalytic cases, no upper limit was used.

The following observations are relevant:

1. Figure 2 depicts the dependence of $\langle c \rangle_\Omega$, over time for various sample sizes, for both the autocatalytic and non-autocatalytic cases. The attained steady state average concentration was roughly double for the autocatalytic case relative to the non-autocatalytic case.
2. Figure 3 depicts the dependence of $\langle \theta \rangle_\Omega$, over time for various sample sizes, for both the autocatalytic and non-autocatalytic cases. The temperature rose to a higher degree in the autocatalytic case, relative to the non-autocatalytic case due to the increased production of the solute, which produces more heat via the reactions, as accounted for by the first law of thermodynamics. Therefore, it was not surprising that the average damage in the material, $\langle \alpha \rangle_\Omega$, was greater in the autocatalytic regime, as depicted in Figure 4.
3. In order to make the stress plots clear, a standard L_2 norm

$$\| \langle \boldsymbol{\sigma} \rangle_\Omega \|^2 \stackrel{\text{def}}{=} (\langle \sigma_{11} \rangle_\Omega)^2 + (\langle \sigma_{22} \rangle_\Omega)^2 + (\langle \sigma_{33} \rangle_\Omega)^2 + (\langle \sigma_{12} \rangle_\Omega)^2 + (\langle \sigma_{13} \rangle_\Omega)^2 + (\langle \sigma_{23} \rangle_\Omega)^2 \quad (21)$$

was taken for illustration purposes (Figure 5). Clearly, in this external pure displacement controlled regime, the stresses relaxed over time, since the material stiffness was being reduced in the interior.

4. In general, the plots for the non-autocatalytic case were 'rougher', relative to the autocatalytic case, because the step sizes had more variability, since they could be made adaptively larger (Figure 6). It is notable that, through variable transformation methods, it is sometimes possible to convert the autocatalytic reaction diffusion equations into standard diffusion forms, which are easier to deal with numerically ([35]). Although transformation techniques were not used in the present analysis, preliminary results found in Reference [36] indicate that they may permit one to use larger time steps when using a backward Euler discretization.
5. The statistical representativeness of the results for the 40 particle sample was also investigated. The procedure was to test 10 samples, each with the same volume fraction of

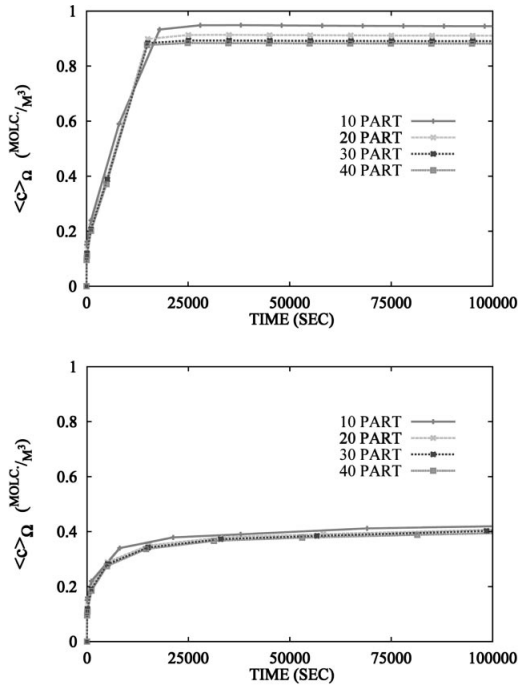


Figure 2. The behaviour of $\langle c \rangle_{\Omega}$ for (top) autocatalytic and (bottom) non-autocatalytic regimes, for 10, 20, 30 and 40 particles per sample. The volume fraction was held constant at approximately 22 per cent volume fraction.

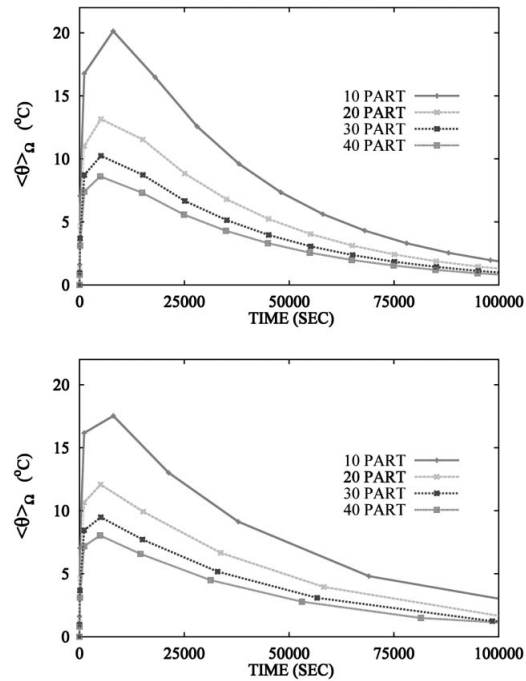


Figure 3. The behaviour of $\langle \theta \rangle_{\Omega}$ for (top) autocatalytic and (bottom) non-autocatalytic regimes, for 10, 20, 30 and 40 particles per sample. The volume fraction was held constant at approximately 22 per cent volume fraction.

spherical particles, but with a different random distribution. The difference between the different 40 particle samples was negligible, and lends credibility that, for the material parameters selected for this numerical study, the results are more or less statistically representative for samples containing approximately 40 particles. Samples containing more particles were tested, with the responses being only minutely different. A more detailed and rigorous analysis of size effects for such systems is beyond the scope of this presentation. The interested reader is referred to a series of works of the materials group at the Ecole Polytechnique Fédérale de Lausanne: Huet [37–41], Huet *et al.* [42], Huet [43–45], Hazanov and Huet [46], Hazanov and Amieur [47], Amieur *et al.* [48], Amieur [49] and Amieur *et al.* [50], as well as some recent work of the author (Zohdi *et al.* [51] or Zohdi and Wriggers [31, 30]).

6. A typical entire simulation for the 40 particle case, such as the ones shown, took no more than 2 h on a high-performance IBM RISC-6000 serial processor, and thus simulations for other parameter selections can be easily performed. The simulation results were compared to the results of the previously mentioned uniform $\Delta t = 10$ s unadaptive unrecursive simulations, with the results being essentially the same. For the recursive adaptive algorithm, the number of multifield system solution solves was uniformly approximately 50 for the

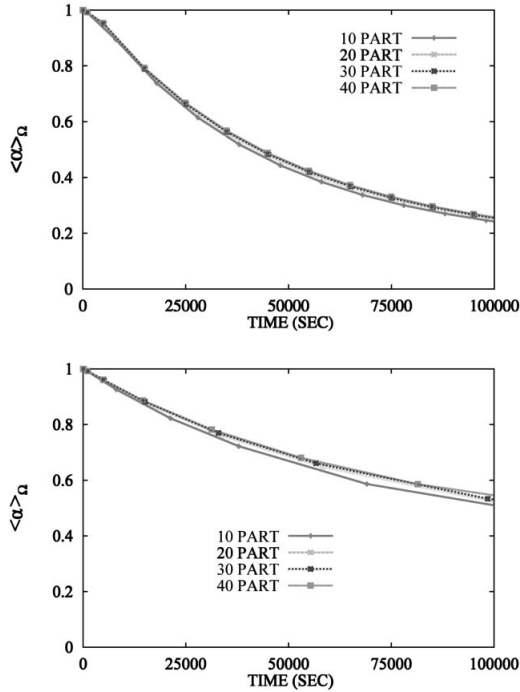


Figure 4. The behaviour of $\langle \alpha \rangle_\Omega$ for (top) autocatalytic and (bottom) non-autocatalytic regimes, for 10, 20, 30 and 40 particles per sample. The volume fraction was held constant at approximately 22 per cent volume fraction.

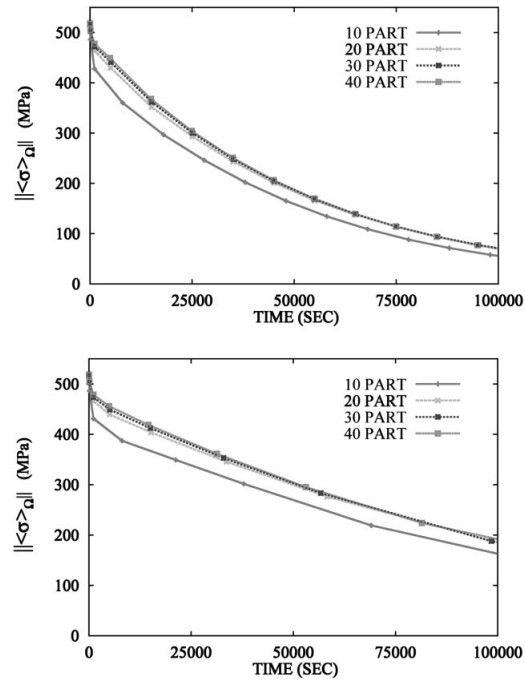


Figure 5. The behaviour of $\| \langle \sigma \rangle_\Omega \|$ for (top) autocatalytic and (bottom) non-autocatalytic regimes, for 10, 20, 30 and 40 particles per sample. The volume fraction was held constant at approximately 22 per cent volume fraction.

Table II. The behavior of quantities of interest with variation in the number of particles per sample, holding the volume fraction constant at approximately 22 per cent. The numerical degrees of freedom shown are for the scalar and the vector-valued problems, respectively.

Part/samp.	Type	DOF	$(\Delta t)^0$	$(\Delta t)^{lim}$	Solves
10	Auto	8000/24 000	10	10 000	52
20	Auto	15 625/46 875	10	10 000	49
30	Auto	24 389/73 167	10	10 000	48
40	Auto	32 768/98 304	10	10 000	49
10	Nonauto	8000/24 000	10	100 000	34
20	Nonauto	15 625/46 875	10	100 000	32
30	Nonauto	24 389/73 167	10	100 000	37
40	Nonauto	32 768/98 304	10	100 000	38

autocatalytic case and uniformly approximately 40 for the non-autocatalytic regime (Table II), as opposed to 10 000 steps with a standard unrecursive, unadaptive, brute force approach.

7. The local damage within the *three-dimensional* microstructure can be observed from orthogonal slices, for progressively increasing time sequences, in Plate 3 for the autocatalytic

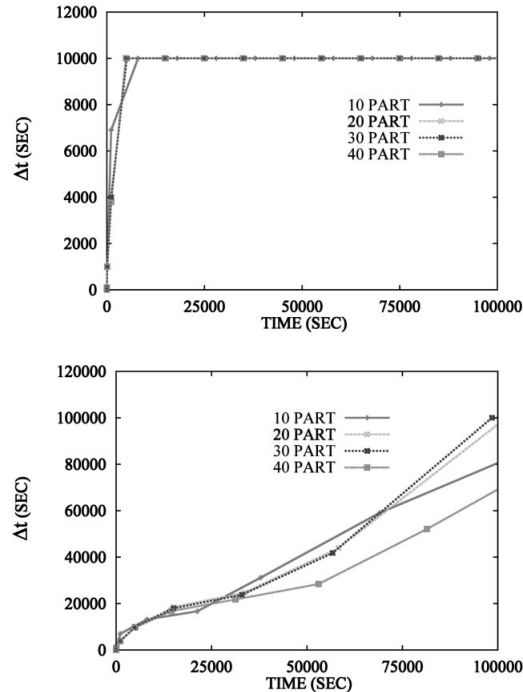


Figure 6. The behaviour of the time step sizes for (top) autocatalytic and (bottom) non-autocatalytic regimes, for 10,20,30 and 40 particles per sample. The volume fraction was held constant at approximately 22 per cent volume fraction.

case, and in Plate 4 for the non-autocatalytic case. Referring to these plates, since the solute concentration was held to unity on the exterior, the damage was higher there, and progressively penetrated into the subsurface. For the autocatalytic case, since the diffusivity of the matrix was selected to be 10 times higher than the diffusivity of the particles, the general trend was that eventually the matrix became more or less uniformly damaged, while the lower diffusivity spherical particles continued to be degraded in a concentric manner. In other words, the solute progressively degraded the particles radially inwards, as exhibited by the 'rings' surrounding the particles. Obviously, the microstructure in the non-autocatalytic case became less damaged in the interior, and exhibited a highly damaged 'crust'. In this case, as dictated by the phenomenological diffusion-reaction equation, the solute reacted and become neutralized ($\tau^0 > 0$). Clearly, for the non-autocatalytic case, the interior became less damaged than the autocatalytic case ($\tau^0 < 0$), which produced more solute in the interior as it further reacted.

5. CONCLUDING REMARKS

The goal of this work was the development of a numerical solution strategy for partial differential equations arising from a description of coupled multifield problems in

microheterogeneous materials. The foundation of the numerical scheme was based upon the observation that a staggering scheme can be written as a fixed-point iteration, whose coupled operator's spectral radius is time step dependent. A sufficient condition for the convergence of such schemes is that the spectral radius of the coupled operator be less than unity. This crucial observation was used to develop a temporally adaptive stepping strategy to maximize the time step sizes, while simultaneously controlling the coupled operator's spectral radius, in order to deliver solutions below an error tolerance within a prespecified number of desired iterations. As illustrated by the numerical examples, it appears possible to achieve accurate solutions at a fraction of the cost of a direct unrecursive, unadaptive, staggering strategy. Therefore, since one cannot usually predict a priori how large a time step should be for accurate solutions, a clear way to use this approach is to start at a very small time step, and to allow the recursive algorithm to adaptively adjust the time steps for a given level of numerical accuracy.

REFERENCES

1. Jikov VV, Kozlov SM, Olenik OA. *Homogenization of Differential Operators and Integral Functionals*. Springer: Berlin, 1994.
2. Aboudi J. *Mechanics of Composite Materials—a Unified Micromechanical Approach*, vol. 29. Elsevier: Amsterdam, 1992.
3. Mura T. *Micromechanics of Defects in Solids* (2nd edn). Kluwer Academic Publishers: Dordrecht, 1993.
4. Nemat-Nasser S, Hori M. *Micromechanics: Overall Properties of Heterogeneous Solids*. Elsevier: Amsterdam, 1993.
5. Park KC, Felippa CA. Partitioned analysis of coupled systems. In *Computational Methods for Transient Analysis*, Belytschko T, Hughes TJR (eds). North-Holland: Amsterdam, 1983.
6. Zienkiewicz OC. Coupled problems and their numerical solution. In *Numerical Methods in Coupled Systems*, Lewis RW, Bettess P, Hinton E (eds). Wiley: Chichester, 1984; 35–58.
7. Schrefler BA. A partitioned solution procedure for geothermal reservoir analysis. *Communications in Applied Numerical Methods* 1985; **1**:53–56.
8. Lewis RW, Schrefler BA, Simoni L. Coupling versus uncoupling in soil consolidation. *International Journal for Numerical and Analytical Methods in Geomechanics* 1992; **15**:533–548.
9. Doltsinis, I. St. Coupled field problems—solution techniques for sequential and parallel processing. In *Solving Large-Scale Problems in Mechanics*, Papadrakakis M (ed.), 1993.
10. Lewis RW, Schrefler BA. *The finite element method in the static and dynamic deformation and consolidation of porous media* (2nd edn). Wiley: New York, 1998.
11. Crank J. *The Mathematics of Diffusion* (2nd edn). Oxford Science Publications: London, 1975.
12. Shewmon PG. *Diffusion in Solids*. McGraw-Hill: New York, 1963.
13. Flynn CP. *Point defects and diffusion*. Clarendon Press: Oxford, 1972.
14. Zohdi TI. Micro-macro modeling, computational testing and design of advanced materials. Habilitation thesis, Universität Hannover, 2001.
15. Kachanov LM. *Introduction to Continuum Damage Mechanics*. Martinus Nijhoff: Dordrecht, 1986.
16. Krajcinovic D. *Damage Mechanics*. North-Holland: Amsterdam, 1996.
17. Lemaitre J, Chaboche J-L. *Mechanics of Solid Materials*. Cambridge University Press: Cambridge, 1990.
18. Axelsson O. *Iterative Solution Methods*. Cambridge University Press: Cambridge, 1994.
19. Perron O. Über Stabilität und asymptotisches Verhalten der Lösungen eines Systems endlicher Differenzengleichungen. *Journal für die Reine und Angewandte Mathematik* 1929; **161**:41–64.
20. Ostrowski A. Les points d' attraction et de répulsion pour l'itération dans l'espace à n dimensions. *Comptes Rendus des séances de l'Académie des Sciences Paris* 1957; **244**:288–289.
21. Ostrowski A. *Solution of Equations and Systems of Equations*. Academic Press: New York, 1966.
22. Ortega J, Rockoff M. Nonlinear difference equations and Gauss–Seidel type iterative methods. *SIAM Journal on Numerical Analysis* 1966; **3**:497–513.
23. Kitchen J. Concerning the convergence of iterates to fixed points. *Studia Mathematica* 1966; **27**:247–249.
24. Ames WF. *Numerical Methods for Partial Differential Equations* (2nd edn). Academic Press: New York, 1977.
25. Southwell RV. *Relaxation Methods in Engineering Science*. Oxford University Press: New York, 1940.
26. Southwell RV. *Relaxation Methods in Theoretical Physics*. Oxford University Press: New York, 1946.
27. Frankel SP. Convergence rates of iterative treatments of partial differential equations. *Math. Tables Aids Comp.* 1950; **4**:65–75.

28. Young DM. Iterative methods for solving partial difference equations of elliptic type. *Doctoral thesis*, Harvard University, 1950.
29. Zohdi TI, Feucht M, Gross D, Wriggers P. A description of macroscopic damage via microstructural relaxation. *International Journal of Numerical Methods in Engineering* 1998; **43**:493–507.
30. Zohdi TI, Wriggers P. Aspects of the computational testing of the mechanical properties of microheterogeneous material samples. *International Journal of Numerical Methods in Engineering* 2001; **50**:2573–2599.
31. Zohdi TI, Wriggers P. On the sensitivity of homogenized material responses at infinitesimal and finite strains. *Communications in Numerical Methods in Engineering* 2000; **16**:657–670.
32. Zohdi TI, Wriggers P. A model for simulating the deterioration of structural-scale material responses of microheterogeneous solids. *Computer Methods in Applied Mechanics and Engineering* 2001; **190**:22–23: 2803–2823.
33. Zohdi TI, Wriggers P. Modeling and simulation of the decohesion of particulate aggregates in a binding matrix. *Engineering Computations* 2001; **18**(1/2):79–95.
34. Zohdi TI. (accepted). Computational optimization of vortex manufacturing of advanced materials. *Computer Methods in Applied Mechanics and Engineering*.
35. Ames WF. *Nonlinear Partial Differential Equations in Engineering*. Academic Press: New York, 1965.
36. Zohdi TI, Wriggers P. (accepted). A Petrov–Galerkin transformation that eliminates spurious oscillations for heterogeneous diffusion-reaction equations. *Computational Materials Science*.
37. Huet C. Remarques sur l'assimilation d'un matériau hétérogène à un milieu continu équivalent. In *Rheological Behaviour and Structure of Materials*, Huet C, Zaoui A (eds). Presses ENPC: Paris, 1981; 231–245.
38. Huet C. Universal conditions for assimilation of a heterogeneous material to an effective medium. *Mechanics Research Communications* 1982; **9**(3):165–170.
39. Huet C. On the definition and experimental determination of effective constitutive equations for heterogeneous materials. *Mechanics Research Communications* 1984; **11**(3):195–200.
40. Huet C. Application of variational concepts to size effects in elastic heterogeneous bodies. *Journal of Mechanics and Physics of Solids* 1990; **38**:813–841.
41. Huet C. Hierarchies and bounds for size effects in heterogeneous bodies. In *Continuum Models and Discrete Systems*, vol. 2, Maugin GA (ed.). 1991; 127–134.
42. Huet C, Navi P, Roelfstra PE. A homogenization technique based on Hill's modification theorem. In *Continuum Models and Discrete Systems*, vol. 2, Maugin GA (ed.). 1991; 135–143.
43. Huet C. In *Activities 1989–1996*, Navi P, Tolou A (eds). Laboratory for Building Materials, Department of Materials Report, 1997.
44. Huet C. An integrated micromechanics and statistical continuum thermodynamics approach for studying the fracture behaviour of microcracked heterogeneous materials with delayed response. *Engineering Fracture Mechanics* (Special issue) 1997; **58**(5–6):459–556.
45. Huet C. Coupled size and boundary condition effects in viscoelastic heterogeneous bodies. *Mechanics of Materials* 1999; **31**(12):787–829.
46. Hazanov S, Huet C. Order relationships for boundary conditions effect in heterogeneous bodies smaller than the representative volume. *Journal of Mechanics and Physics of Solids* 1994; **42**:1995–2011.
47. Hazanov S, Amieur M. On overall properties of elastic heterogeneous bodies smaller than the representative volume. *International Journal of Engineering Science* 1995; **33**(9):1289–1301.
48. Amieur M, Hazanov S, Huet C. Numerical and experimental study of size and boundary conditions effects on the apparent properties of specimens not having the representative volume. In *Micromechanics of Concrete and Cementitious Composite*, Huet C (ed.), 1993.
49. Amieur M. Etude numérique et expérimentale des effets d'échelle et de conditions aux limites sur des éprouvettes de béton n'ayant pas le volume représentatif, Doctoral dissertation No. 1256, Ecole Polytechnique Fédérale de Lausanne, Lausanne, Switzerland, 1994.
50. Amieur M, Hazanov S, Huet C. Numerical and experimental assessment of the size and boundary conditions effects for the overall properties of granular composite bodies smaller than the representative volume. In *IUTAM Symposium on Anisotropy, Inhomogeneity and Nonlinearity in Solid Mechanics*, Parker DF, England AH (eds). Kluwer Academic Publishers: The Netherlands, 1995; 149–154.
51. Zohdi TI, Wriggers P, Huet C. A method of substructuring large-scale computational micromechanical problems. *Computer Methods in Applied Mechanics and Engineering* (accepted).